Supporting Information for *Acta Phys. -Chim. Sin.* doi: 10.3866/PKU.WHXB202205012

单离子聚合物快离子导体

薛国勇[1,2]，李静[2]，陈俊超[3]，陈代前[2]，胡晨吉[2,3]，唐凌飞[1,2]，陈博文[1,2]，易若玮[2]，沈炎宾[1,2,*]，陈立桅[2,3,*]

[1]中国科学技术大学纳米技术与纳米仿生学院，合肥 230026

[2]中国科学院苏州纳米技术与纳米仿生研究所，创新实验室卓越纳米科学中心，江苏苏州 215123

[3]上海交通大学化学化工学院，上海 200240

A Single-Ion Polymer Superionic Conductor

Guoyong Xue [1,2], Jing Li [2], Junchao Chen [3], Daiqian Chen [2], Chenji Hu [2,3], Lingfei Tang [1,2], Bowen Chen [1,2], Ruowei Yi [2], Yanbin Shen [1,2,*], Liwei Chen [2,3,*]

[1] School of Nano-Tech and Nano-Bionics, University of Science and Technology of China, Hefei 230026, China.

[2] i-Lab, CAS Center for Excellence in Nanoscience, Suzhou Institute of Nano-Tech and Nano-Bionics, Chinese Academy of Science, Suzhou, 215123, Jiangsu Province, China.

[3] School of Chemistry and Chemical Engineering, Shanghai Jiaotong University, Shanghai 200240, China

[*]Corresponding authors. Emails: ybshen2017@sinano.ac.cn (Y.S.); lwchen2018@sjtu.edu.cn (L.C.).

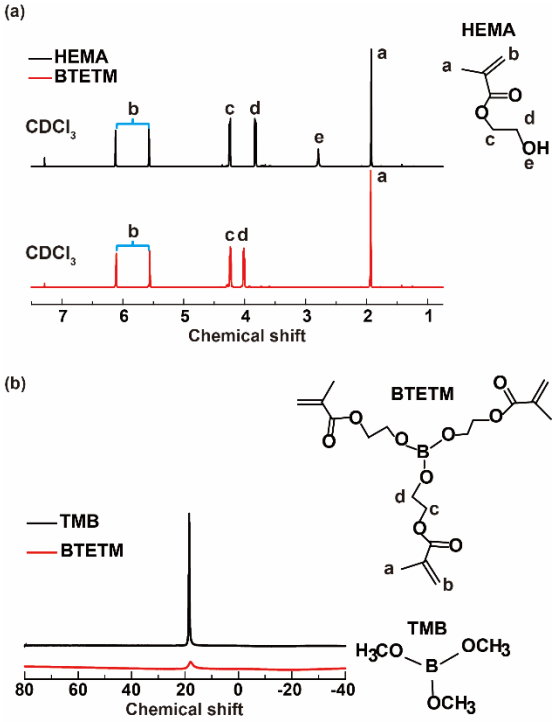

Fig. S1 (a) ^{1}H-NMR spectra of the HEMA and BTETM samples. (b) ^{11}B-NMR of the TMB and BTETM samples.

The structure of the synthesized BTETM was characterized by nuclear magnetic resonance (NMR), It is obvious that when the hydroxyl groups of the HEMA are substituted, the hydroxyl resonance peak of e disappears, while the resonance peak of d shifts from the original 3.82 to 4.01 due to the lack of electrons in the boron atom. In addition, both TMB and BTETM exhibit a resonance peak near 18.0, which belongs to the tri-coordinated boron atoms, but the resonance peak of the BTETM is much broader than that of the TMB due to the different coordination molecules of the tri-coordinated boron atoms. These results confirm the successful synthesis of the BTETM.

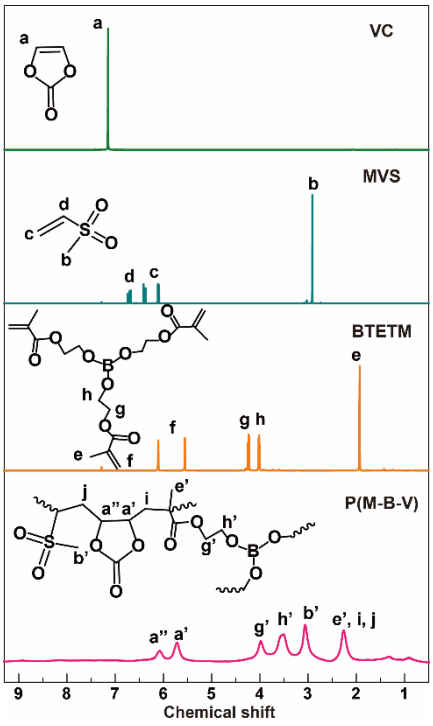

Fig. S2 ^{1}H-NMR spectra of the VC, MVS, BTETM, and P(M-B-V).

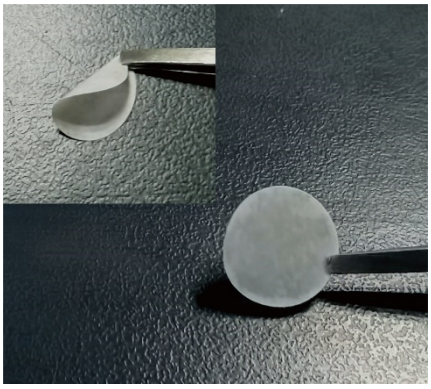

Fig. S3 Optical image of the P(M-B-V) membrane.

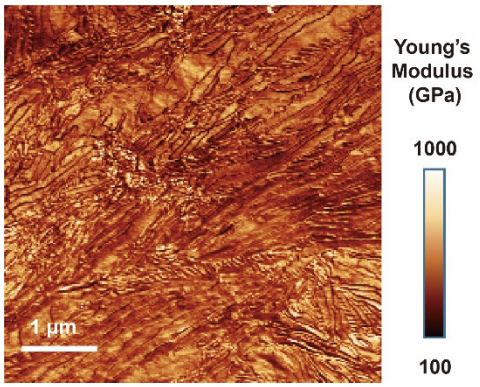

Fig. S4 AFM Young's modulus mapping of the PEO SPE.

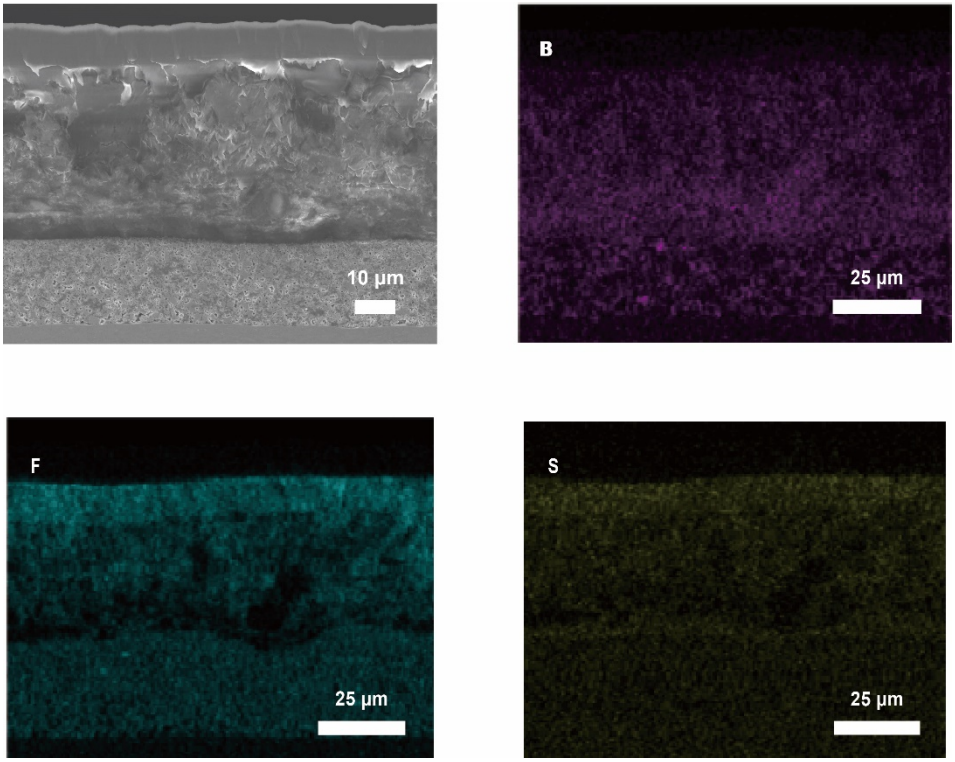

Fig. S5 The cross-sectional SEM image of the P(M-B-V) and corresponding EDX elemental mapping (B, F, and S).

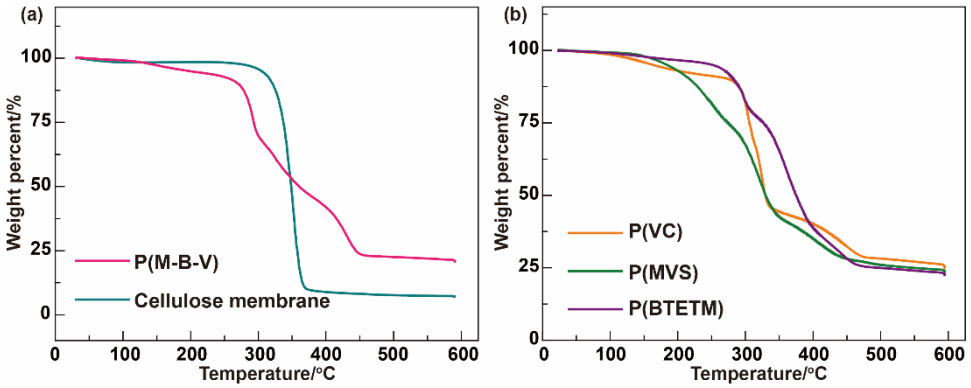

Fig. S6 (a-b) Thermogravimetric curves of the cellulose membrane, P(M-B-V), P(VC), P(MVS) and P(BTEME).

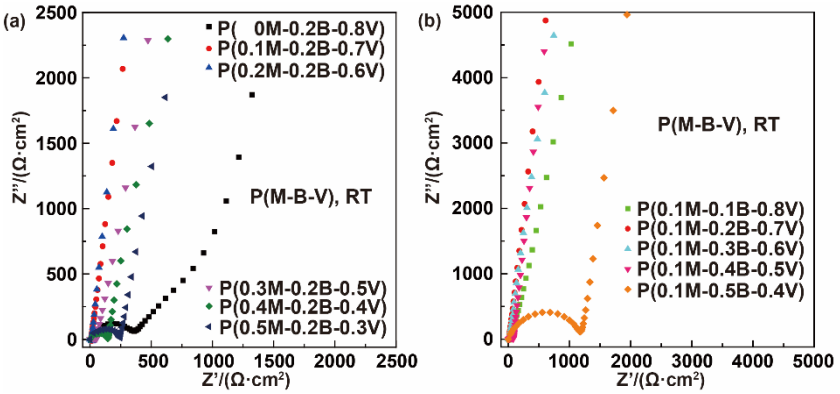

Fig. S7 (a–b) Nyquist plots of the P(M-B-V) SPEs with different weight fractions of MVS, BTETM and VC measured at RT.

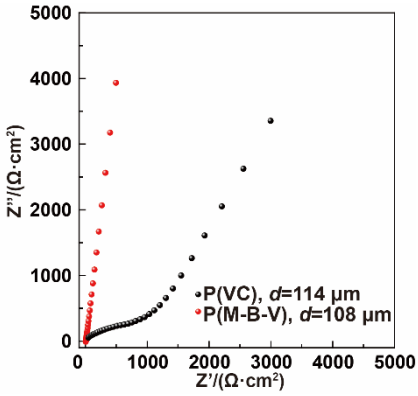

Fig. S8 Nyquist plots of the P(VC) and P(M-B-V) measured at RT.

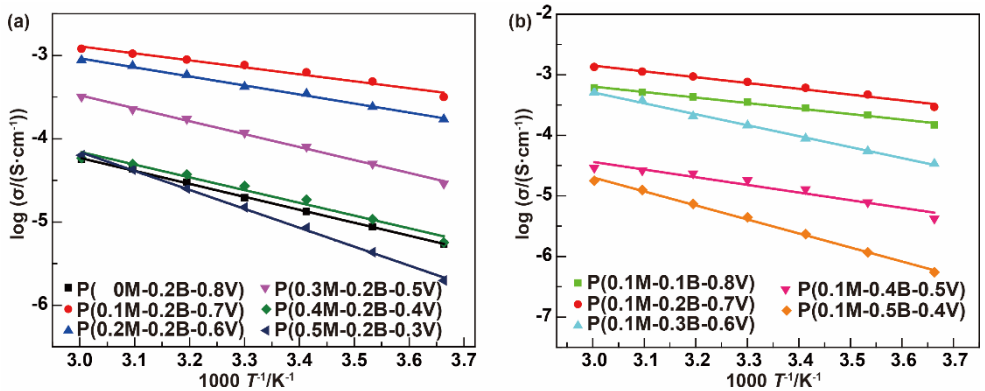

Fig. S9 (a–b) Arrhenius plots at temperatures from 0 to 60 °C for the P(M-B-V) SPEs with different weight fractions of MVS, BTETM, and VC.

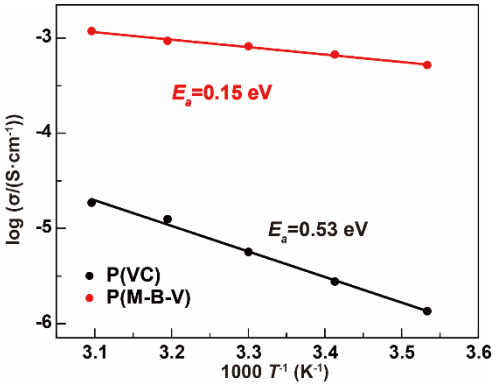

Fig. S10 Arrhenius plots at temperatures from 10 °C to 50 °C for the P(VC) and P(M-B-V).

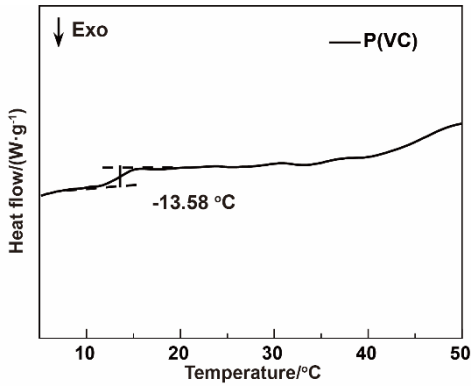

Fig. S11 DSC curve of the P(VC).

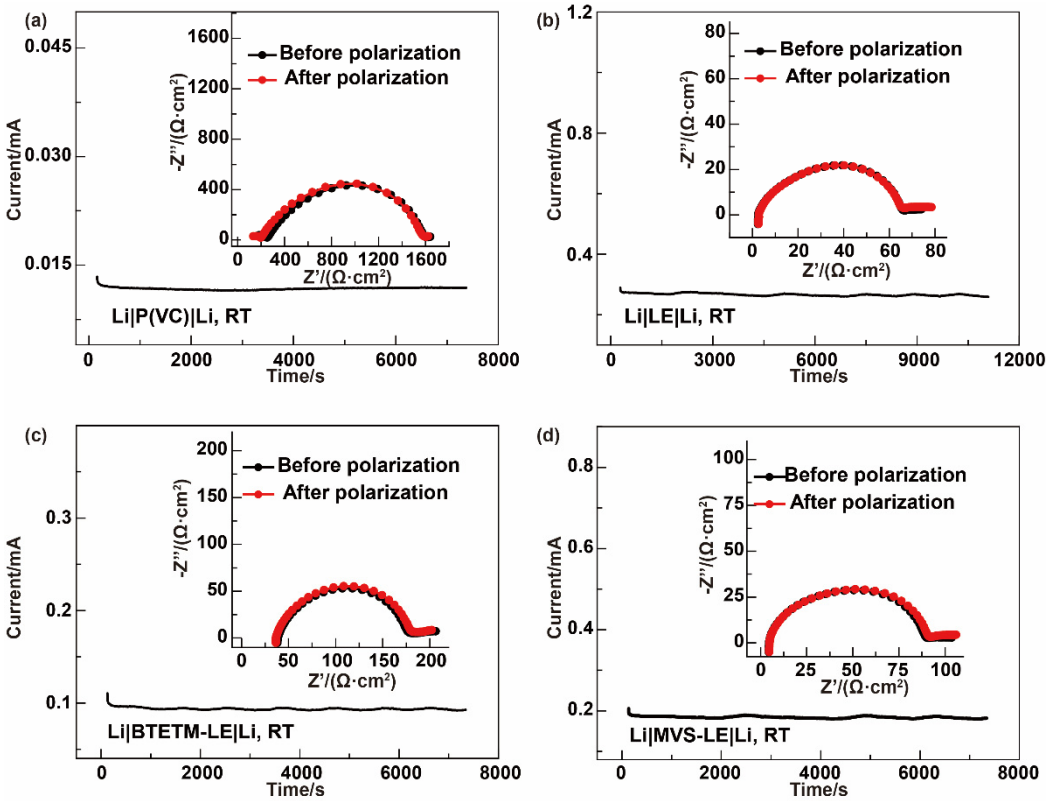

Fig. S12 (a–d) Current-time plots with Nyquist plots before and after polarization (inset) of symmetric Li cells with P(VC), liquid, BTETM-liquid and MVS-liquid electrolytes.

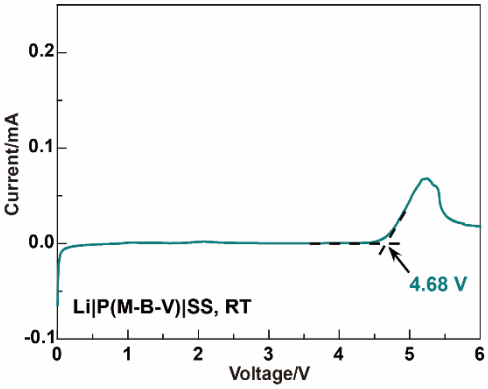

Fig. S13 Linear sweep voltammetry (LSV) curve of the P(M-B-V).

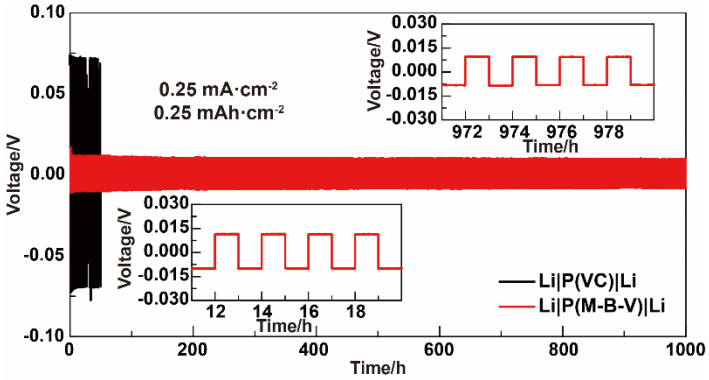

Fig. S14 Li plating/stripping cycling of symmetric Li cells containing P(VC) (black) and P(M-B-V) SISC (red) at a current density of 0.25 mA·cm^{-2} for 1 h at RT. The insets show magnified curves at the indicated time periods.

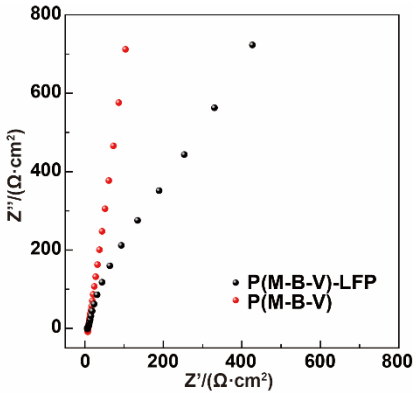

Fig. S15 Nyquist plots of the P(M-B-V)-LFP (the weight fraction of P(M-B-V) in the cathode is approximately 0.22%–0.25%) and the P(M-B-V) SISC.

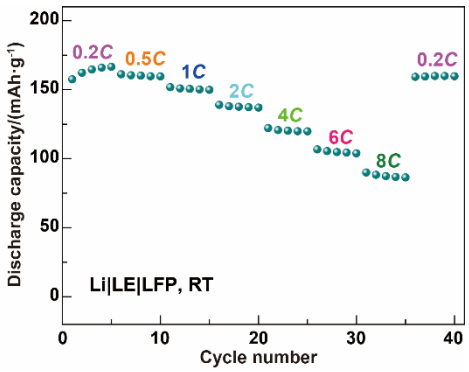

Fig. S16 Rate capability of Li||LFP batteries with liquid electrolyte at RT.

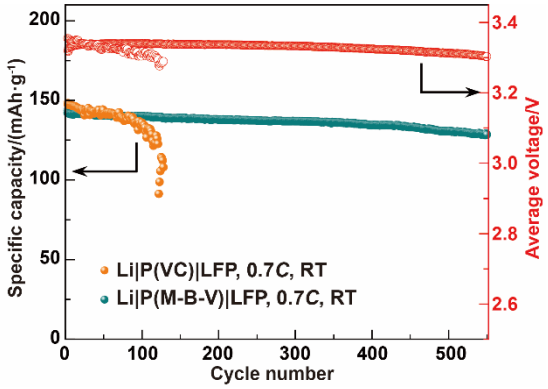

Fig. S17 Cycling performance of Li||LFP batteries with the P(M-B-V) SISC (dark cyan) and the P(VC) (orange) at 0.7*C*, RT.

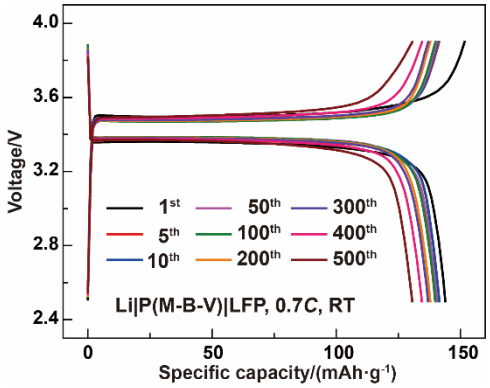

Fig. S18 Voltage profile evolution of the Li|P(M-B-V)|LFP battery cycled 0.7*C*, RT.

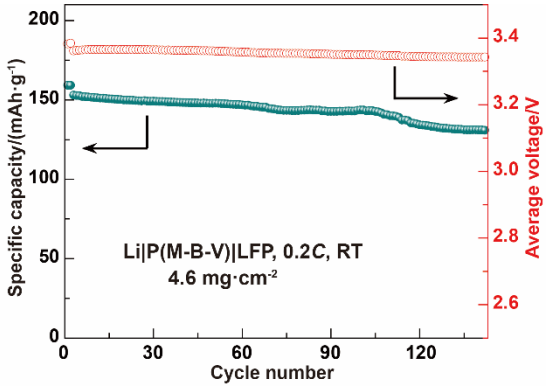

Fig. S19 Cycling performance of Li|P(M-B-V)|LFP battery with cathode areal loading as high as 4.6 mg·cm^{-2} at 0.2*C*, RT.

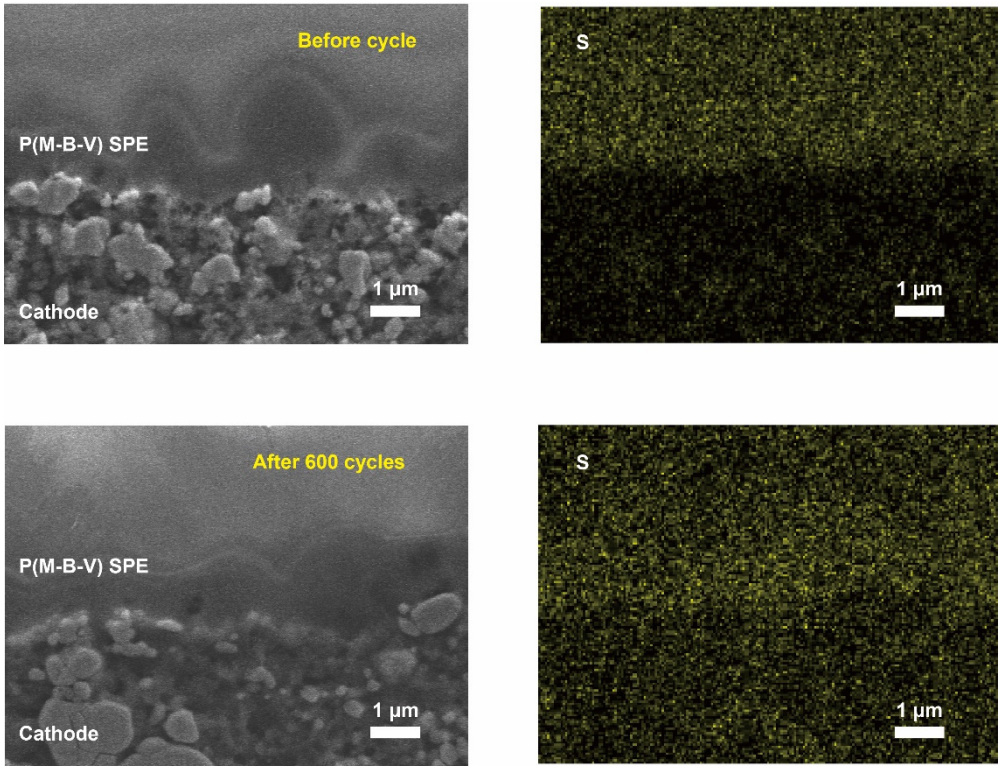

Fig. S20 SEM image and EDX elemental mapping (S) of the interface between the LFP cathode and the P(M-B-V) SISC before and after 600 cycles.

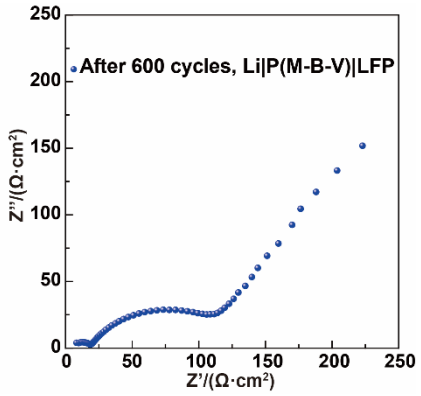

Fig. S21 Nyquist plot of the Li|P(M-B-V)|LFP battery after 600 cycles.

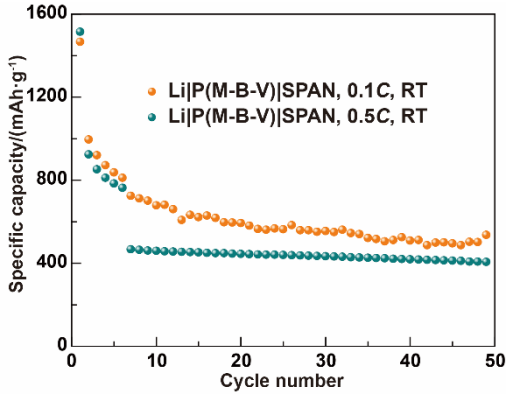

Fig. S22 Cycling performance of the Li|P(M-B-V)|SPAN batteries at 0.1*C* and 0.5*C* (activating at 0.05*C* for 6 cycles before the cycling).

Table S1 Lithium-ion transference number and the ambient ionic conductivity of the P(M-B-V) SPEs with different weight fractions of MVS, BTETM and VC.

	BTETM	MVS	VC	σ/(mS·cm^{-1})	t_{Li+}
1	0.2	0.0	0.8	0.021	0.63
2	0.2	0.1	0.7	1.290	0.94
3	0.2	0.2	0.6	0.353	0.67
4	0.2	0.3	0.5	0.096	0.88
5	0.2	0.4	0.4	0.055	0.78
6	0.2	0.5	0.3	0.038	0.82
7	0.1	0.1	0.8	0.945	0.90
8	0.3	0.1	0.6	0.489	0.80
9	0.4	0.1	0.5	0.119	0.68
10	0.5	0.1	0.4	0.005	0.58

Table S2 Lithium-ion transference number of the P(M-B-V), P(VC), liquid, BTETM-liquid and MVS-liquid electrolytes.

	R_0/Ω	R_S/Ω	I_0/mA	I_S/mA	t_{Li+}
P(M-B-V)	333.1	354.6	0.0297	0.0279	0.94
P(VC)	674.0	692.0	0.0134	0.0119	0.48
LE	32.22	32.22	0.2890	0.2580	0.36
B-LE	69.79	72.72	0.1100	0.0926	0.60
M-LE	43.96	44.95	0.2050	0.1820	0.48

Table S3 Performance comparison of the P(M-B-V) SISC and the P(M-B-V) based solid state battery with recent works.

Material	Electrolyte type	$\sigma \times 10^4$ at room temperature (S·cm^{-1})	t_{Li+}	Tensile stress/MPa	Cycle performance(battery-*C* rate-temperature-cycles-capacity retention)	Ref
B-PEG@DMC	Solid polymer electrolyte (SPE)	0.23	–	–	LFP/Li-0.2*C*-25 °C-100th-73%	1
SLIMs	Gel polymer electrolyte (GPE)	0.27	0.62	0.40	LFP/Li-0.1*C*-25 °C -150th-80%	2
NPEs	SPE	0.32	0.47	1.60	LFP/Li-0.5*C*-25 °C -100th-92%	3
CPSHPE	SPE	0.89	0.26	0.43	LFP/Li-0.1*C*-30 °C-70th-87.7%	4
PBI-g-LiPSTFSI	GPE	1.50	0.91	14.50	LFP/Li-1*C*-25 °C-500th-87%	5
ANP-5	GPE	1.50	0.95	–	LFP/Li-0.5*C*-30 °C-100th-84%	6
PVDF/PP	SPE	1.53	0.24	7.05	LFP/Li-0.3*C*-25 °C-180th-97.8%	7
LITFSI/PUA	SPE	0.03	–	11.1	LFP/Li-0.03*C*-25 °C-20th	8
PAS/PS	SPE	0.54/60 °C	0.96	–	LFP/Li-0.2*C*-25 °C-60th-88.1%	9
IN-SCPEs	SPE	1.90	0.90	0.50	LFP/Li-0.5*C*-28 °C-200th-83.2%	10
PIL-PEO	SPE	6.00	0.22	–	LFP/Li-0.5*C*-55 °C-50th-77%	11
SHCPE	Composite polymer electrolyte (CPE)	0.80	0.43/60 °C	0.12	LFP/Li-0.2*C*-60 °C-60th-95.8%	12
P(M-B-V) SISC	**SPE**	**12.90**	**0.94**	**13.10**	**LFP/Li-0.5*C*-30 °C-630th-90%**	**This work**

References

(1) Li, R. Y.; Hua, H. M.; Zeng, Y. J.; Yang, J.; Chen, Z. Q.; Zhang, P.; Zhao, J. B. *J. Energy Chem.* **2022**, *64*, 395. doi: 10.1016/j.jechem.2021.04.037

(2) Guan, X.; Wu, Q. P.; Zhang, X. W.; Guo, X. H.; Li, C. L.; Xu, J. *Chem. Eng. J*. **2020**, *382*, 122935. doi: 10.1016/j.cej.2019.122935

(3) Dong, L. N.; Zeng, X. F.; Fu, J. F.; Chen, L. Y.; Zhou, J.; Dai, S. W.; Shi, L. Y. *Chem. Eng. J*. **2021**, *423*, 130209. doi: 10.1016/j.cej.2021.130209

(4) Zhou, B. H.; Yang, M. L.; Zuo, C.; Chen, G.; He, D.; Zhou, X. P.; Liu, C. M.; Xie, X. L.; Xue, Z. G. *ACS Macro Lett*. **2020**, *9*, 525. doi: 10.1021/acsmacrolett.9b01024

(5) Du, D. D.; Li, H. J.; Xu, H.; Zhang, Y. F.; Sun, Y. B.; Zeng, D. L.; Cheng, H. S. *J. Alloy. Compd*. **2021**, *881*, 160573. doi: 10.1016/j.jallcom.2021.160573

(6) Shin, D. M.; Bachman, J. E.; Taylor, M. K.; Kamcev, J.; Park, J. G.; Ziebel, M. E.; Velasquez, E.; Jarenwattananon, N. N.; Sethi, G. K.; Cui, Y.; Long, J. R. *Adv. Mater*. **2020**, *32*, 1905771. doi: 10.1002/adma.201905771

(7) Shi, K.; Xu, Z. J.; Huang, M. Q.; Zou, L.; Zheng, D. W.; Yang, Z. H.; Zhang, W. X. *J. Membr. Sci*. **2021**, *638*, 119713. doi: 10.1016/j.memsci.2021.119713

(8) Mendes-Felipe, C.; Barbosa, J. C.; Goncalves, R.; Miranda, D.; Costa, C. M.; Vilas-Vilela, J. L.; Lanceros-Mendez, S. *J. Energy Chem*. **2021**, *62*, 485. doi: 10.1016/j.jechem.2021.01.030

(9) Hu, T. X.; Shen, X.; Peng, L. Q.; Liu, Y. Z.; Wang, X.; Ma, H. S.; Zhang, P.; Zhao, J. B. *J. Phys. Chem. Solids* **2021**, *158*, 110229. doi: 10.1016/j.jpcs.2021.110229

(10) Guan, T. Y.; Rong, Z. L.; Cheng, F. Y.; Zhang, W. Q.; Chen, J. *ACS Appl. Energ. Mater*. **2020**, *3*, 12532. doi: 10.1021/acsaem.0c02483

(11) Li, Y. H.; Sun, Z. J.; Shi, L.; Lu, S. Y.; Sun, Z. H.; Shi, Y. C.; Wu, H.; Zhang, Y. F.; Ding, S. J. *Chem. Eng. J*. **2019**, *375*, 121925. doi: 10.1016/j.cej.2019.121925

(12) Zhou, B. H.; Jo, Y. H.; Wang, R.; He, D.; Zhou, X. P.; Xie, X. L.; Xue, Z. G. *J. Mater. Chem. A* **2019**, *7*, 10354. doi: 10.1039/c9ta01214a